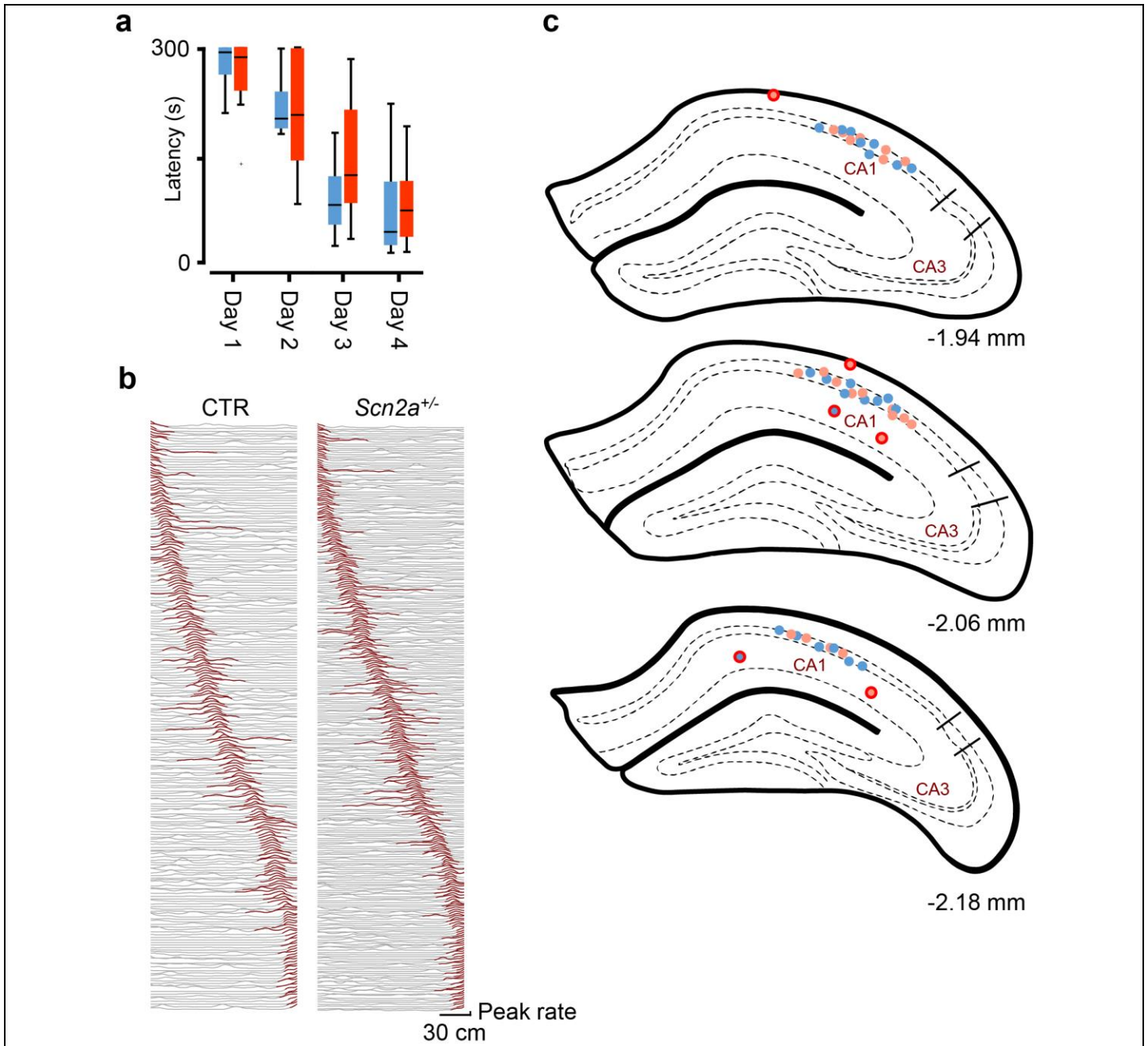


In the format provided by the authors and unedited.

Altered hippocampal replay is associated with memory impairment in mice heterozygous for the *Scn2a* gene

Steven J. Middleton ^{1,2*}, Emily M. Kneller¹, Shuo Chen^{1,2}, Ikuo Ogiwara^{3,4}, Mauricio Montal ⁵, Kazuhiro Yamakawa ^{2,3*} and Thomas J. McHugh ^{1,2,6*}

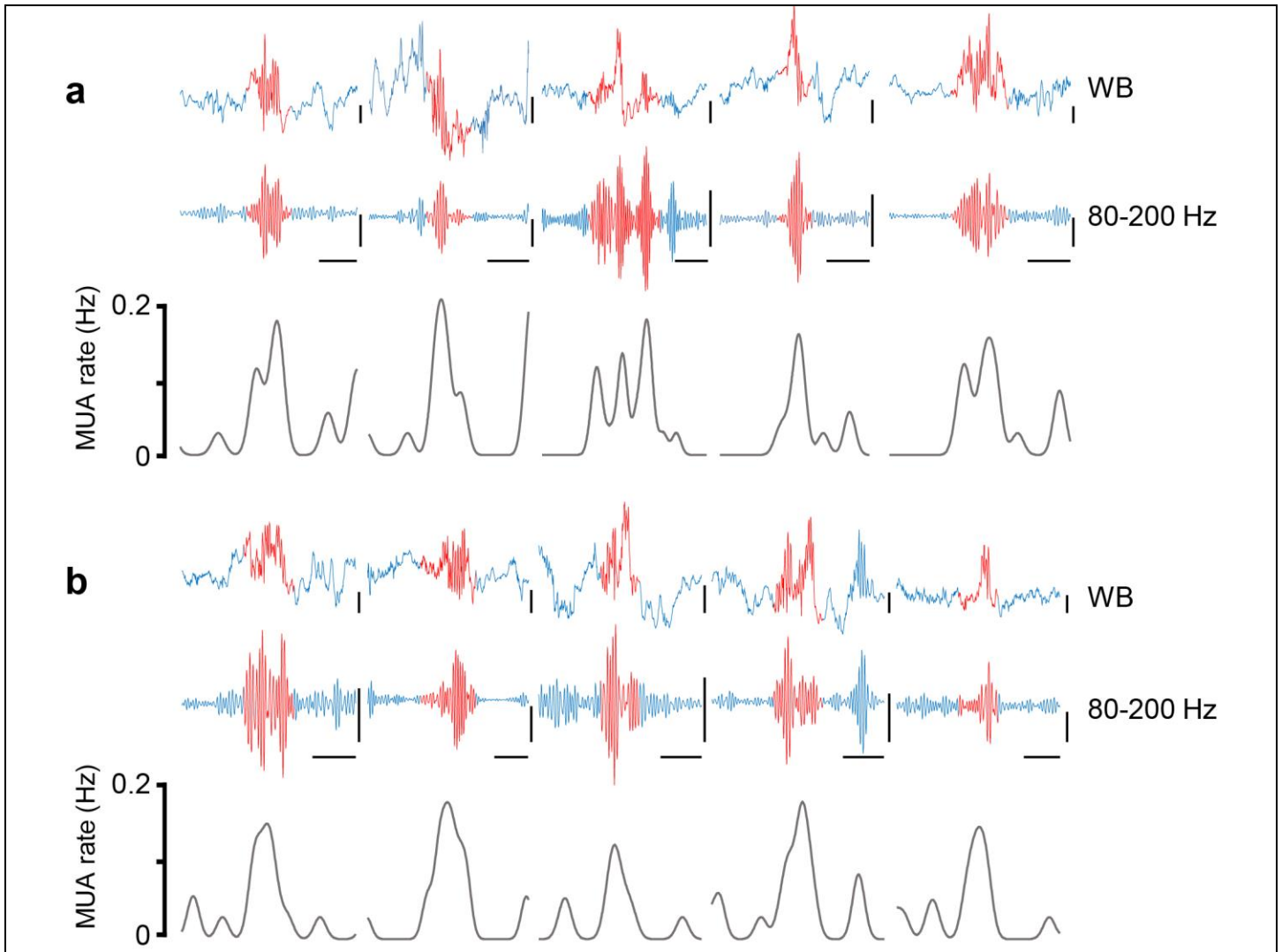
¹Laboratory for Circuit and Behavioral Physiology, RIKEN Brain Science Institute, Wakoshi, Saitama, Japan. ²RIKEN Center for Brain Science, Wakoshi, Saitama, Japan. ³Laboratory for Neurogenetics, RIKEN Brain Science Institute, Wakoshi, Saitama, Japan. ⁴Department of Physiology, Nippon Medical School, Tokyo, Japan. ⁵Section of Neurobiology, University of California San Diego, California, La Jolla, USA. ⁶Department of Life Sciences, Graduate School of Arts and Sciences, University of Tokyo, Tokyo, Japan. *e-mail: stevenmiddleton@brain.riken.jp; yamakawa@brain.riken.jp; thomas.mchugh@riken.jp



Supplementary Figure 1

Spatial learning, place fields and tetrode locations.

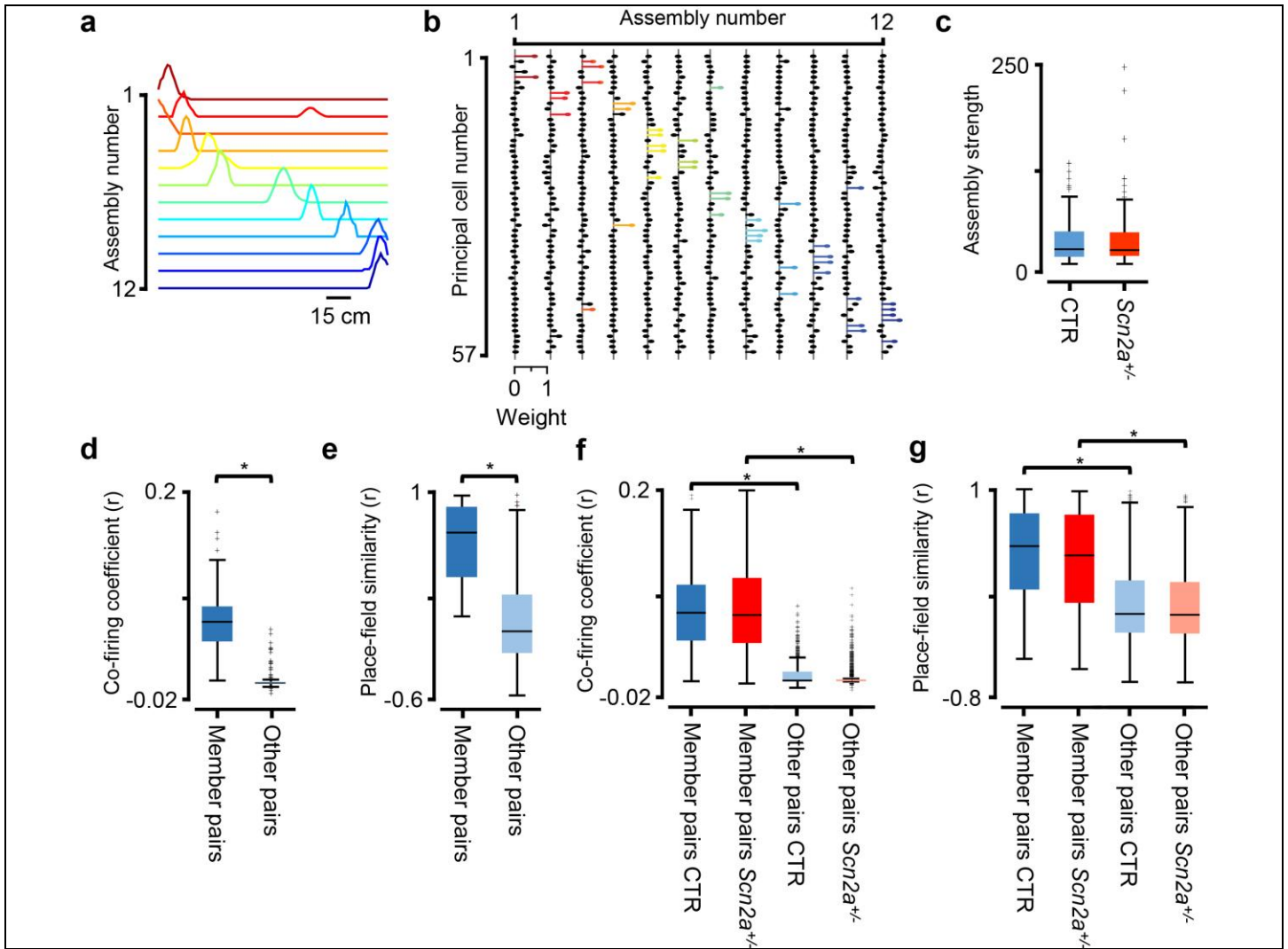
(a) Latencies during Barnes maze learning over a four day period revealed control mice (blue) learned faster than *Scn2a*^{+/-} mice (red) ($P=0.0027$, $F=5.19$, 2-way repeated measures ANOVA, followed by post-hoc Bonferroni test $P<0.01$ on day 3; CTR: $N=14$ animals; SCN: $N=14$ animals). (b) The spatial receptive fields are shown for all recorded place cells during linear track exploration sessions. Individual grey lines represent single place cell rate maps across the entirety of the track, dark red areas indicate place fields determined as described in the methods section. Control (left) and *Scn2a*^{+/-} (right) fields are ordered according to their peak position on the track. (c) Reconstructed tetrode tip locations from three animals of each genotype (blue CTR, pink *Scn2a*^{+/-}) overlaid onto schematic mouse brain slices, numbers indicate posterior distances from bregma. Tetrodes circled in red were excluded as they were either poorly targeted or were devoid of place cells. All boxplots represent the median (black line) and the 25th-75th percentiles, with whiskers extending to the most extreme data points, excluding outliers which are plotted as individual crosses. * $P < 0.05$.



Supplementary Figure 2

Sharp wave ripple event detection.

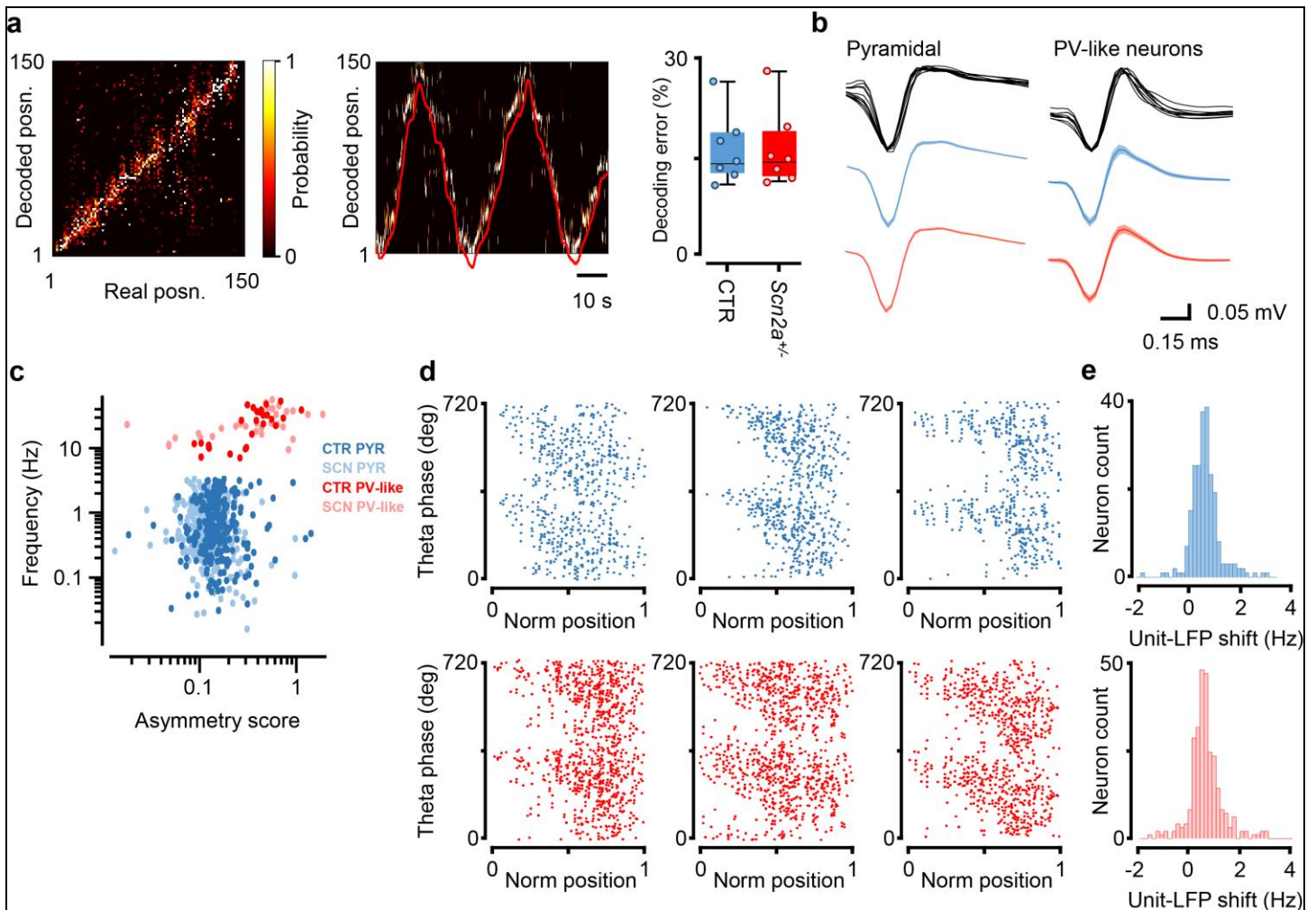
(a) Upper traces (WB) show five examples of raw CA1 *stratum pyramidale* local field potentials recorded from control mice during a rest period in a small sleep box. Blue traces represent activity centered on events detected as SPW-Rs, with the period detected as a ripple (as described in the methods section) highlighted in red. Below these are the same LFPs band-pass filtered between 80-200 Hz. The bottom panel shows multi-unit activity of all clustered place cells for the corresponding time periods. (b) Shows the same but for *Scn2a*^{+/-} mice. Scale bars represent 100 ms (horizontal) and 100 μ V (vertical) throughout.



Supplementary Figure 3

Detection of cell assemblies.

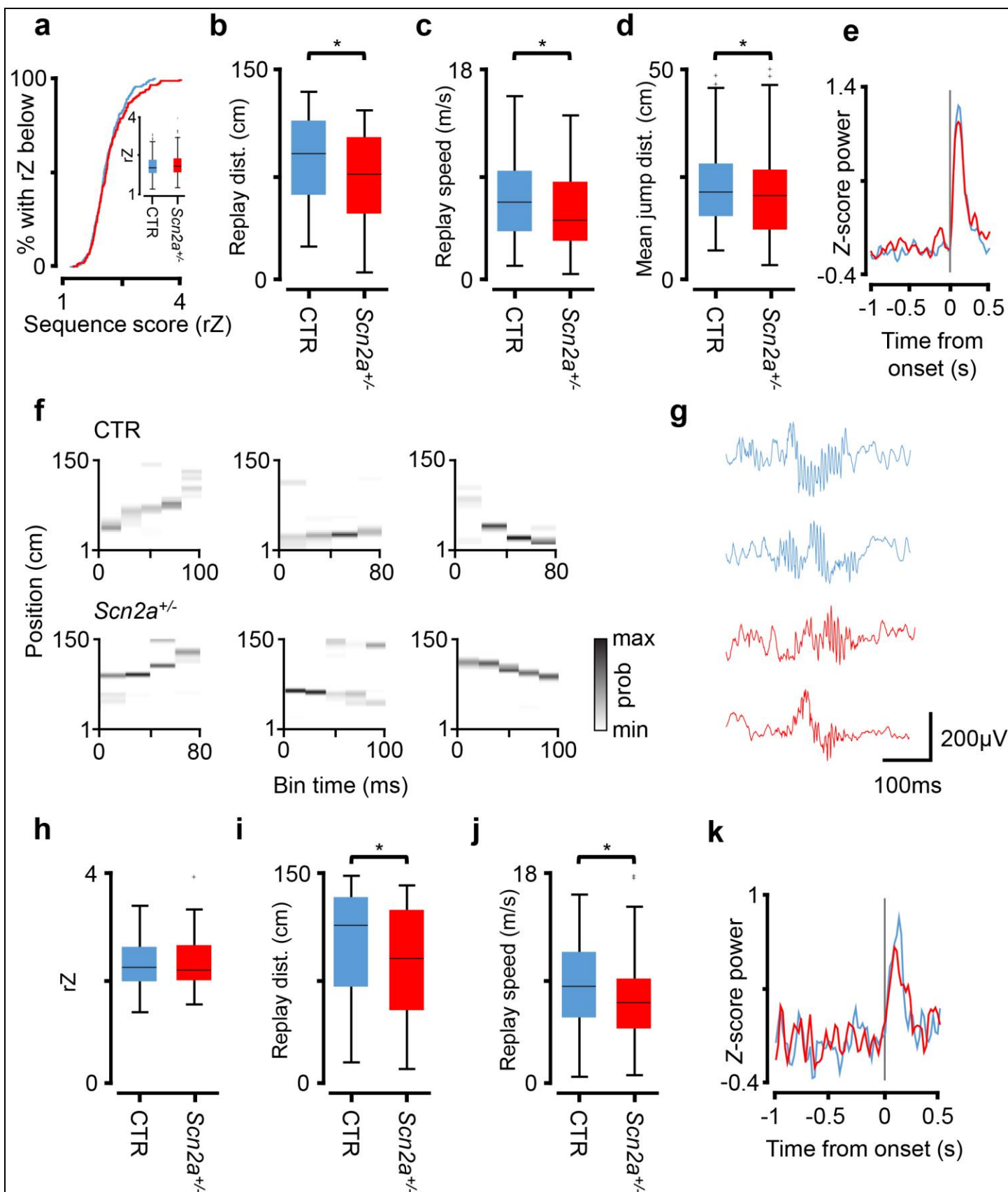
(a) Session example showing assembly spatial maps (of 12 cell assemblies) ordered from left to right across the entirety of the linear track. (b) Corresponding data showing the 57 CA1 place cells recorded during this session, each neurons weight in a given assembly is indicated by its deviation on the x-axis. Cells with a significant weight are color coded to the assembly to which they belong (from a). (c) Mean assembly strength during linear track exploration did not differ between genotypes ($P=0.83$, $Z=0.22$, two-sided Wilcoxon Rank-sum; CTR: $N=7$ animals, $n=96$ cell assemblies; SCN: $N=7$ animals, $n=132$ cell assemblies). (d) Cells classified as forming part of an assembly had significantly higher co-firing coefficients (r) with assembly partners, than cells which did not form part of any assembly ($P=3.32 \times 10^{-23}$, $Z=9.92$, two-sided Wilcoxon Rank-sum; $n=59$ assembly cell pairs, $n=105$ non-assembly cell pairs), relating to example session shown in a & b. (e) Place-field similarity was also significantly greater for assembly member pairs, compared with non-members ($P=1.62 \times 10^{-16}$, $Z=8.25$, two-sided Wilcoxon Rank-sum; $n=59$ assembly cell pairs, $n=105$ non-assembly cell pairs). (f) Across all subjects during SPW-Rs, cell pairs forming part of an assembly had consistently higher co-firing coefficients independent of genotype (CTRs, $P=1.28 \times 10^{-52}$, $Z=15.3$, two-sided Wilcoxon Rank-sum; SCN, $P=7.82 \times 10^{-67}$, $Z=17.3$, two-sided Wilcoxon Rank-sum; CTR: $N=7$ animals; SCN: $N=7$ animals), when compared to non-members. (g) Place field similarity was also significantly higher for cell-assembly members for both controls ($P=1.25 \times 10^{-21}$, $Z=9.55$, two-sided Wilcoxon Rank-sum, $N=7$ animals) and mutants ($P=4.31 \times 10^{-25}$, $Z=10.3$, two-sided Wilcoxon Rank-sum, $N=7$ animals). Cell-assembly members ($P=0.31$, $Z=1.02$, two-sided Wilcoxon Rank-sum; CTR: $N=7$ animals; SCN: $N=7$ animals) and non-members ($P=0.73$, $Z=0.35$, two-sided Wilcoxon Rank-sum; CTR: $N=7$ animals; SCN: $N=7$ animals) were not significantly different when compared across genotype. All boxplots represent the median (black line) and the 25th-75th percentiles, with whiskers extending to the most extreme data points, excluding outliers which are plotted as individual crosses. * $P < 0.05$.



Supplementary Figure 4

Spike waveforms and Bayesian decoding of position.

(a) Left panel shows decoding accuracy for a full linear track exploration session, with hot colors indicating highest probabilities and high probabilities along the diagonal demonstrating decoded positions accurately reflect the real world position of the animal. Middle panel shows multiple traversals of the linear track using the Bayesian decoder, hot colors representing highest probability, red line indicates true position and is shifted vertically for clarity. Right panel shows the mean decoding error for both control (blue) and *Scn2a*^{+/-} mice (red), with individual points representing single animals ($P=0.99$, two-sided Wilcoxon Rank-sum; CTR: $N=7$ animals; SCN: $N=7$ animals). (b) Example spike waveforms recorded from control mice in CA1 *stratum pyramidale*, for both neurons classified as both pyramidal cells (top left) and parvalbumin-like interneurons (top right). Middle panel (blue) shows average waveforms for all pyramidal (left) and PV-like (right) neurons from control mice. *Scn2a*^{+/-} average waveforms are shown in the bottom panel (red) with pyramidal left and PV-like to the right, shaded areas represent SEM. (c) Pyramidal (blue) and PV-like neurons (red) were separable into two distinct clusters based on waveform asymmetry and firing frequency, however within cell types, genotypes (control and *Scn2a*^{+/-} are represented by dark and light colors respectively) were indistinguishable. (d) Example phase precession plots for three place cells from each genotype (control and *Scn2a*^{+/-} in blue and red respectively), showing spikes moving to progressively earlier phases with increasing passage into place fields. (e) Histograms showing the relative frequency of all place cells relative to LFP theta, with positive values indicate phase precession of cells ($P=0.24$, $Z=1.16$, two-sided Wilcoxon Rank-sum; CTR: $N=7$ animals, $n=224$ cells; SCN: $N=7$ animals, $n=274$ cells). All boxplots represent the median (black line) and the 25th-75th percentiles, with whiskers extending to the most extreme data points, excluding outliers which are plotted as individual crosses. * $P < 0.05$.



Supplementary Figure 5

Awake replay events are truncated in a similar manner to sleep replays.

(a) Cumulative distribution of sequence scores (rZ) for events detected by both MUA and ripple power, the means \pm SEM are displayed in the inset ($P=0.33$, $Z=0.98$, two-sided Wilcoxon Rank-sum; CTR: $N=7$ animals, $n=241$ events; SCN: $N=7$ animals, $n=255$ events). (b) Group data showing mean distances spanned by replay events detected by a combination of both MUA and ripple power ($P=2.4 \times 10^{-5}$, $Z=4.23$, two-sided Wilcoxon Rank-sum; CTR: $N=7$ animals, $n=241$ events; SCN: $N=7$ animals, $n=255$ events). (c) Average speed in m/s of progression from starting position to end position for all replay events detected by MUA and ripple power ($P=4.1 \times 10^{-4}$, $Z=3.5$, two-sided Wilcoxon Rank-sum; CTR: $N=7$ animals, $n=241$ events; SCN: $N=7$ animals, $n=255$ events). (d) The average spatial jump in centimeters for decoded positions in adjacent temporal bins, for each replay event ($P=0.016$, $Z=2.41$, two-sided Wilcoxon Rank-sum; CTR: $N=7$ animals, $n=241$ events; SCN: $N=7$ animals, $n=255$ events). (e) Mean z-scored LFP ripple power concurrent with all significant replay events, lined up to the time of initial detection of the events (CTR: $N=7$ animals, $n=241$ events; SCN: $N=7$ animals, $n=255$ events), control (blue) and *Scn2a*^{+/-} (red) are represented by their respective colors throughout (a-e). (f) Examples of trajectory sequences derived from Bayesian decoding of spiking activity during awake SPW-Rs, top row represents controls, beneath are *Scn2a*^{+/-} examples. (g) Representative examples of unfiltered SPW-Rs during the awake exploratory session, for both control (blue) and *Scn2a*^{+/-} (red). (h) Mean replay event sequence scores (rZ) for control (blue) and *Scn2a*^{+/-} (red) in the awake exploratory session ($P=0.97$, $Z=0.03$, two-sided Wilcoxon Rank-sum; CTR: $N=7$ animals, $n=59$ events; SCN: $N=7$ animals, $n=88$ events). (i) Group data showing mean distances spanned by awake replay events detected by a combination of both MUA and ripple power ($P=0.044$, $Z=2.0$, two-sided Wilcoxon Rank-sum; CTR: $N=7$ animals, $n=59$ events; SCN: $N=7$ animals, $n=88$ events). (j) Average speed in m/s of progression from starting position to end position for all awake replay events detected by MUA and ripple power ($P=0.027$, $Z=2.2$, two-sided Wilcoxon Rank-sum; CTR: $N=7$ animals, $n=59$ events; SCN: $N=7$ animals, $n=88$ events). (k) Mean z-scored LFP ripple power concurrent with all significant awake replay events, lined up to the time of initial detection (combined ripple power and MUA), control and *Scn2a*^{+/-} are represented by blue and red respectively (CTR: $N=7$ animals, $n=59$ events; SCN: $N=7$ animals, $n=88$ events). All boxplots represent the median (black line) and the 25th-75th percentiles, with whiskers extending to the most extreme data points, excluding outliers which are plotted as individual crosses. * $P < 0.05$.

Supplementary Table 1 Behavior, unit and LFP properties

	Control	SCN2A ^{+/-}	P-value
Ripple properties	(N=7)	(N=7)	
Rate	0.38±0.03 Hz	0.42±0.02 Hz	0.54 (WRS)
Ripples with significant sequences	8.9±3.2 %	5.7±1.1 %	0.46 (WRS)
Concatenated Length	131.2±19.4 ms	127.0±6.3 ms	0.71(WRS)
LFP properties	(N=7)	(N=7)	
Theta frequency	8.7±0.3 Hz	9.0±0.2 Hz	0.49 (WRS)
Animal behavior	(N=7)	(N=7)	
Velocity	8.1±0.3 cm/s	7.6±0.5 cm/s	0.36 (WRS)
Completed laps	10.1±1.6	9.6±1.3	0.87 (WRS)
Stops/lap	0.07±0.03	0.14±0.04	0.21 (WRS)
Lap duration	23.3±2.4 s	27.3±3.0 s	0.3 (WRS)
Place cell properties	(n=229)	(n=282)	
Percentage of all cells	83.8±2.5 %	86.4±2.2%	0.6 (WRS)
Peak in-field rate	4.1±0.2 Hz	4.2±0.2 Hz	0.81 (WRS)
Number of fields/cell	1.2±0.03	1.2±0.04	0.41 (WRS)
Firing rate (exploration session)	0.70±0.03 Hz	0.69±0.03 Hz	0.85 (WRS)
Firing rate (sleep session excluding SPW-Rs)	0.70±0.04 Hz	0.62±0.03 Hz	0.09 (WRS)
Firing rate (sleep session during SPW-Rs)	0.94±0.05 Hz	0.70±0.03 Hz	0.00002 (WRS)
Ripple participation	12.6±0.6%	10.2±0.41%	0.002 (WRS)
PV-like properties	(n=23)	(n=34)	
Firing rate (exploration session)	19.4±2.3 Hz	21.5±1.8 Hz	0.5 (WRS)
Firing rate (sleep session excluding SPW-Rs)	11.4±1.1 Hz	14.1±0.9 Hz	0.11 (WRS)
Firing rate (sleep session during SPW-Rs)	20.3±4.5 Hz	28.2±3.6 Hz	0.028 (WRS)
Ripple participation	69.3±5.3%	84.5±3.3%	0.07

N denotes number of animals, n denotes number of cells, WRS signifies a two-sided Wilcoxon Rank-sum test and data are presented as means ± s.e.m.